Physics of Fluids

RESEARCH ARTICLE | JANUARY 11 2024

Numerical investigation on non-linear streaming effects in a two-stage coaxial pulse tube cryocooler

Damu C ; Sumukh Moudghalya ; Mrunal M. Nerale ; Debashis Panda ; Rajendra Prasad K S ; Upendra Behera ; B. N. Sathyanarantana Reddy

Physics of Fluids 36, 016124 (2024)
https://doi.org/10.1063/5.0178688

Numerical investigation on non-linear streaming effects in a two-stage coaxial pulse tube cryocooler

Cite as: Phys. Fluids **36**, 016124 (2024); doi: 10.1063/5.0178688
Submitted: 28 September 2023 · Accepted: 8 December 2023 ·
Published Online: 11 January 2024

Damu C,[1] Sumukh Moudghalya,[2] Mrunal M. Nerale,[2] Debashis Panda,[2] Rajendra Prasad K S,[3,a)] Upendra Behera,[2] and B. N. Sathyanarantana Reddy[1]

AFFILIATIONS

[1]Department of Mechanical Engineering, Sambhram Institute of Technology, Bangalore 560097, India
[2]Centre for Cryogenic Technology, Indian Institute of Science, Bangalore, India
[3]Department of Mechanical and Industrial Engineering, Manipal Institute of Technology Bengaluru, Manipal Academy of Higher Education, Manipal 560064, India

[a)]Author to whom correspondence should be addressed: rajendra.prasad@manipal.edu

ABSTRACT

Stirling pulse tube cryocoolers (PTC) are widely used in aerospace applications for the cooling of infrared sensors and for filtering background thermal noise in the astro-imaging devices, etc. Present investigation aims to use numerical methods to demonstrate the nonlinear fluid flow, heat transfer, and vortex generation phenomena in a two-stage coaxial type inertance pulse tube cryocooler. The numerical simulation is conducted using commercially available Fluent® code for both single-stage and multi-stage configurations to show nonlinear processes with varying heat load conditions. It has been noticed that the width of the vortex produced inside the pulse tube grows with an increase in heat load capacity. This undesirable flow conditions yields an adverse effect in the cooling behavior and reduces overall performance of cryocooler with higher heat load. Additionally, streamlines, stream function, pressure and temperature variation plots are given for both stages with different heat load capacity to substantiate our results.

NOMENCLATURE

C_2	inertial resistance (m^{-1})
D_h	hydraulic diameter (m)
E_f	fluid specific energy (J/kg)
E_s	solid specific energy (J/kg)
f	frequency (Hz)
k	thermal conductivity (W/m K)
n_g	porosity
P	Pressure (Pa)
P_a	Pressure amplitude (Pa)
P_{in}	Pressure inlet (Pa)
P_o	mean pressure (Pa)
t	time (s)
T	Temperature (K)
v_r	radial velocity (m/s)
v_z	axial velocity (m/s)

Greek symbols

α	permeability (m^2)
β	viscous resistance (m^{-2})
ρ_s	solid density (kg/m^3)
ρ_f	fluid density (kg/m^3)
$\bar{\bar{\tau}}$	stress tensor (N/m^2)

Abbreviations

CFD	computational fluid dynamics
PTC	pulse tube cryocooler

I. INTRODUCTION

Cryocoolers have become essential components in various fields such as electronics cooling, space exploration, and medical equipment. Among various types of cryocoolers, the pulse tube cryocooler (PTC) has received significant attention due to its advantages such as compactness, reliability, and absence of moving parts in the low-temperature section.[1,2] The PTC operates on the principle of Stirling cycle, which involves the compression and expansion of gas parcels within the closed system.[1] The PTC uses a pulse tube to transfer the heat from the cold end to the warm end of the device. This heat

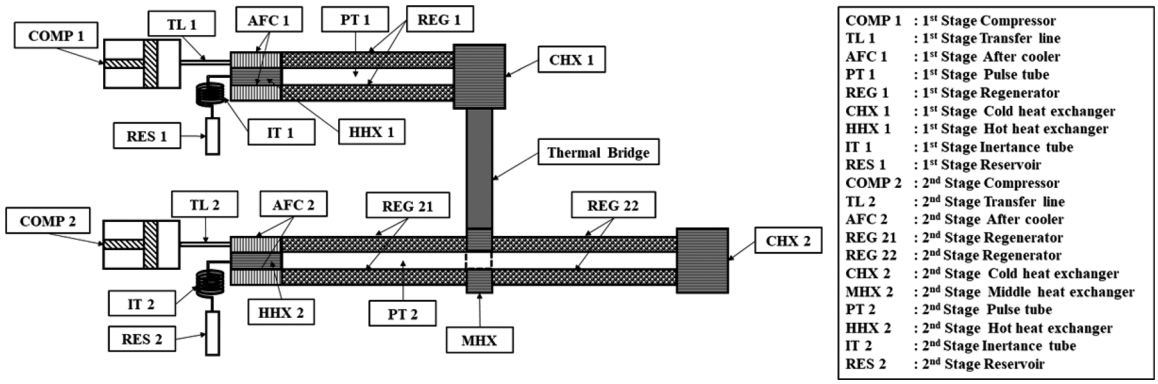

FIG. 1. Schematics of a thermally coupled two-stage coaxial pulse tube cryocooler.

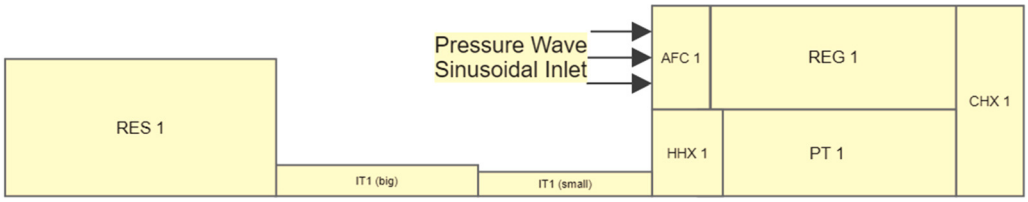

(a) Axisymmetric geometry of the first-stage of PTC.

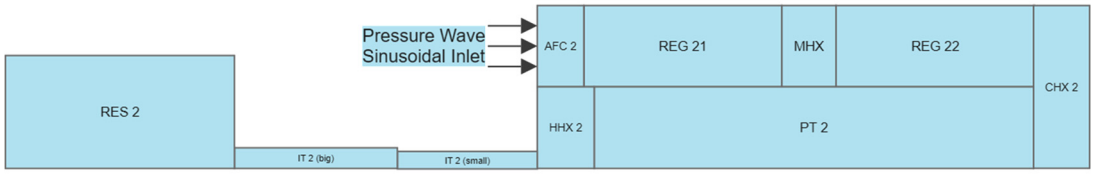

(b) Axisymmetric geometry of the second-stage of PTC.

FIG. 2. (a) Axisymmetric geometry of the first-stage of PTC. (b) Axisymmetric geometry of the second-stage of PTC.

transfer is achieved through the use of a phase-shifted oscillation between the flow rate and pressure within the pulse tube and regenerator. In addition, the PTC has been used in space applications due to its ability to operate without any moving parts in the cold section, hence making it ideal for environments with low levels of vibration.[1] The performance enhancement of PTCs has been the topic of much research and development throughout the past years. As a result, improvements have been made in crucial areas, such as reliability, cooling capacity, and efficiency. Improvement in regenerator design and packing processes,[3,4] development of novel regenerator materials,[5,6] and optimization in geometries[7,8] are a few steps to enhance its thermodynamic performance. These developments have produced PTCs with cooling capacities ranging from 0.1 W to 10 kW that can achieve temperatures as low as 4 kelvins for several practical applications.

Rapid use of cryocoolers in aerospace and space satellite cooling applications stimulates cryocooler researchers to reduce their physical shape and size, thus, different configurations like inline, coaxial, annular, etc. have been proposed.[1] The coaxial configuration is one of the simplest configurations and is mostly preferred for satellite cooling application in space. The cold head is concentrically positioned within the warm part of the coaxial PTC, and the annular space between them is filled with screen meshes which functions like a regenerator. This coaxial structure has a number of benefits, including a small footprint and a high surface area of heat transfer between the working gas

TABLE I. Geometrical details of the first-stage of coaxial PTC.[a]

Components	Outer radius (mm)	Inner radius (mm)	Length (mm)
Aftercooler	12	7	20
Regenerator	12	7	64
Cold heat exchanger	12	7	10
Pulse tube	···	7	76
Hot heat exchanger	···	7	8
Inertance tube 1	···	1.75	2800
Inertance tube 2	···	2.25	1400
Reservoir	···	30	80

[a]The cold heat exchanger, pulse tube, hot heat exchanger, inertance tube 1, inertance tube 2, and reservoir are circular. So its inner radius is equal to the radius. Wall thickness is neglected for all the components.

TABLE II. Geometrical details of the second-stage of coaxial PTC.[a]

Components	Outer radius (mm)	Inner radius (mm)	Length (mm)
Aftercooler	10	6	12
Regenerator 1	10	6	40
Middle heat exchanger	10	6	8
Regenerator 2	10	6	30
Cold heat exchanger	10	6	10
Pulse tube	⋯	6	80
Hot heat exchanger	⋯	6	10
Inertance tube 1	⋯	1.5	3200
Inertance tube 2	⋯	2.25	1200
Reservoir	⋯	30	80

[a]The cold heat exchanger, pulse tube, hot heat exchanger, inertance tube 1, inertance tube 2, and reservoir are circular. So its inner radius is equal to the radius. Wall thickness is neglected for all the components.

TABLE III. Optimized meshing details of both stages of computational domain.

Model	Cells	Nodes
First stage PTC	44 960	54 385
Second stage PTC	50 860	59 863

TABLE IV. Thermal boundary conditions for each computational domain.

Components	Boundary condition
Aftercooler, hot heat exchanger	Isothermal (300 K)
Middle heat exchanger (second stage only)	45 K
Cold heat exchanger	Heat flux values depending upon heat load[a]
Regenerator, Pulse tube, Inertance tube, Reservoir	Adiabatic

[a]Simulation happened for three different heat load values of 0.6, 1.8, and 3.0 W in first-stage. The heat load values for the second-stage are 0.8, 2.4, and 4 W, respectively.

and regenerator to improve its cooling efficiency. However, the presence of gas streaming effects and dispersion mechanisms within the pulse tube can decline its performance and cooling efficiency.[9–14] In this paper, we aim to provide a comprehensive overview on those gas streaming effects for both single-stage and multistage PTC by showcasing the flow streamlines for varying cold end loads through computational fluid dynamics (CFD) simulations. Through our analysis, the vortices are observed inside the pulse tube with different heat loads for both single-stage and two-stage PTC.

Gas streaming is used to describe the non-ideal behavior of gas flow inside the pulse tube, which can lead to unfavorable outcomes like unwanted temperature gradients, pressure loss, and energy losses.[9] One of the adverse effects of gas streaming is the occurrence of disturbed heat flow along the pulse tube through the axial heat conduction. As the gas oscillates within the pulse tube, thermal energy can be conducted along the length of the tube, thus leading to temperature gradients. These temperature gradients can affect the efficiency of the PTC by reducing the temperature difference between hot and cold ends, thus limiting the cooling capacity. Another gas streaming effect is pressure drop, which is caused by viscous dissipation. As the gas flows through the porous zones of regenerator, frictional forces between the gas molecules and the tube screen meshes result in energy loss due to viscous dissipation, thermal dissipation and pressure drop.[15] This pressure drop can impact the overall performance of the PTC by reducing the pressure amplitude and increasing the input power required for gas compression. Furthermore, the presence of boundary layer effects can affect the gas flow patterns within the pulse tube. Boundary layers are formed near the walls of the pulse tube due to the no-slip boundary condition where gas molecules adhere to the tube surface. These boundary layers can impede the gas flow, leading to an increase in gas resistance and decrease in heat transfer efficiency.[16–18] However, the physical visualization of such oscillating phenomena is quite impossible as it happens in a stainless steel pipe. This needs specialized neutron imaging visualization techniques to accurately detect those streamlines. The accuracy of visualization by neutron imaging method also raises doubts due to the rapid gas flow process inside pulse tubes as a result of high oscillating frequencies. With the use of computational modeling and simulations techniques, such as Computational Fluid Dynamics (CFD), these effects can be better understood through detailed scientific visualization and interpretation of the mitigating gas streamlines. CFD simulation allows for the analysis of these complex flow phenomena and aid in optimizing pulse tube designs to minimize the pressure drops, and energy losses.

Prior research in this field indicates the effect of parameters such as geometry and frequency on these vortex formation mechanisms. However, those articles neglected the impact of heat loads on the shapes of non-linearity in streamlines.[9,12,13,19] This paper focuses on the computational analysis of flow streaming effects inside the pulse tube subjected to external heat loads at cold end, which is one of the most important factors in practical conditions. The analysis is conducted for both single-stage and two-stage PTC in order to analyze the differences in streaming patterns, which can be taken up for further studies.

TABLE V. Values of inertial resistance and viscous resistance for the porous zones of PTC.

Component	Porosity	Inertial resistance (1/m)	Viscous resistance ($1/m^2$)	Material (mesh no.)
Regenerator 1	0.6858	3.41890×10^4	2.08333×10^{10}	SS #400
Regenerator 2	0.607	5.17070×10^4	4.16667×10^{10}	SS #500
Hot heat exchanger	0.691	7883	1.29870×10^9	Cu #100
Cold heat exchanger	0.691	6905	1.29870×10^9	Cu #100

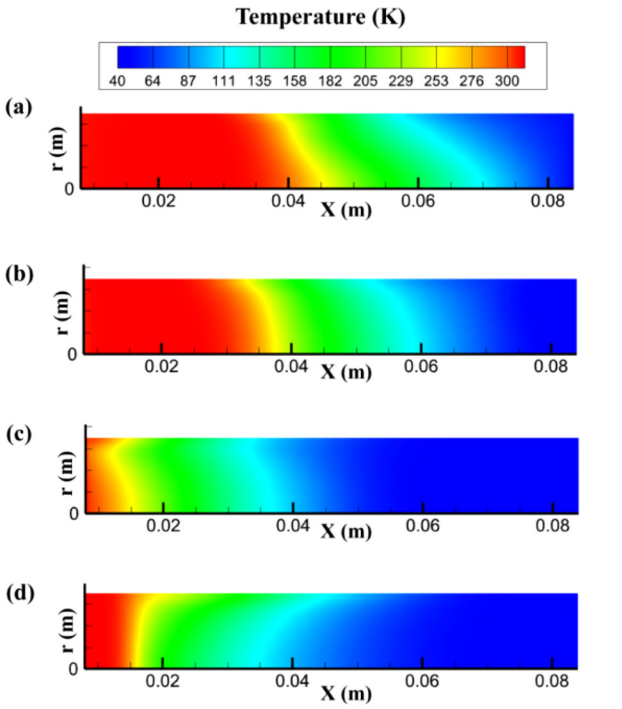

FIG. 3. Temperature contour within the pulse tube for 0.6 W of heat load for a phase angle of (a) 0°, (b) 90°, (c) 180°, and (d) 270°.

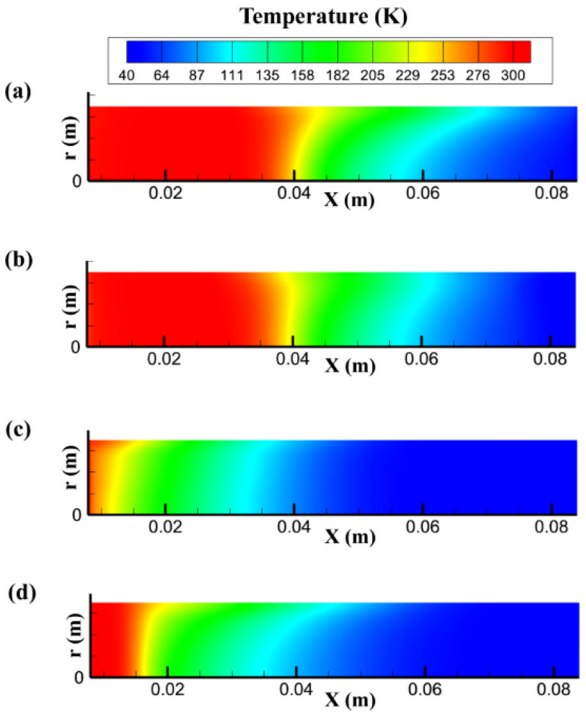

FIG. 5. Temperature contour within the pulse tube for 3 W of heat load for a phase angle of (a) 0°, (b) 90°, (c) 180°, and (d) 270°.

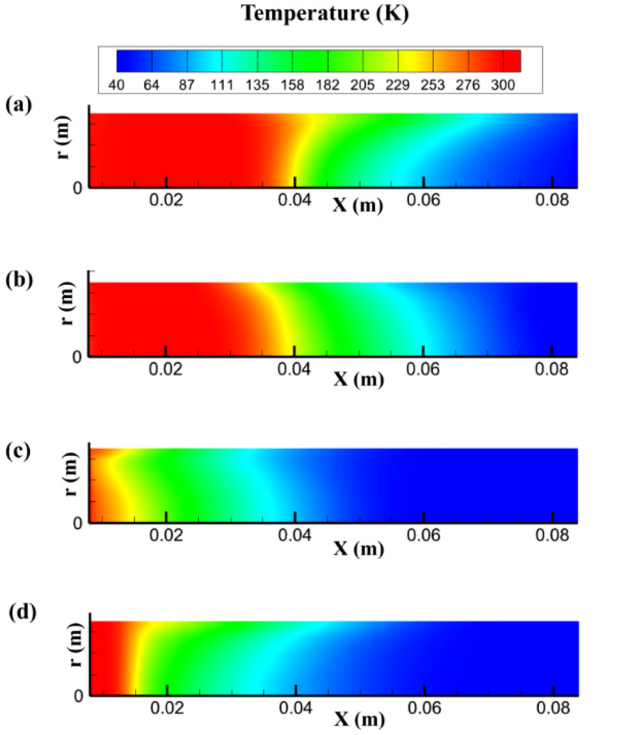

FIG. 4. Temperature contour within the pulse tube for 1.8 W of heat load for a phase angle of (a) 0°, (b) 90°, (c) 180°, and (d) 270°.

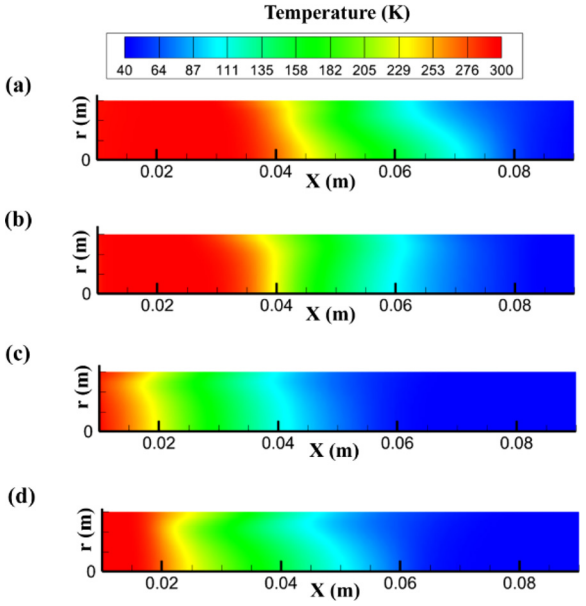

FIG. 6. Temperature contour inside the second-stage pulse tube for 0.8 W heat loads for a phase angle of (a) 0°, (b) 90°, (c) 180°, and (d) 270°.

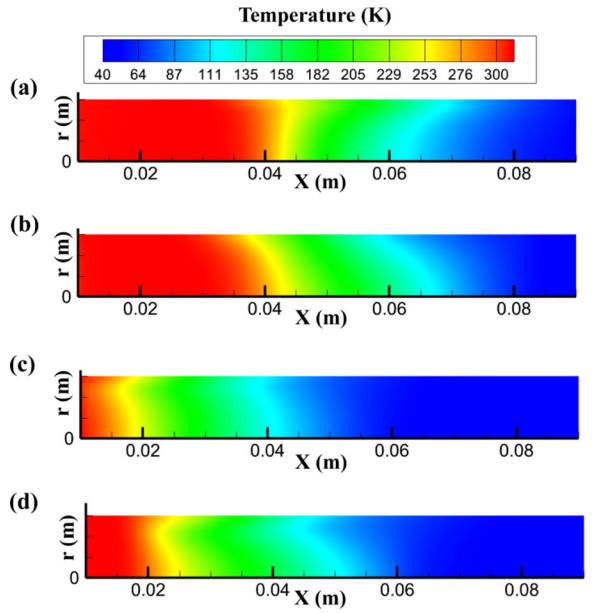

FIG. 7. Temperature contour inside the second-stage pulse tube for 2.4 W heat loads for a phase angle of (a) 0°, (b) 90°. (c) 180°, and (d) 270°.

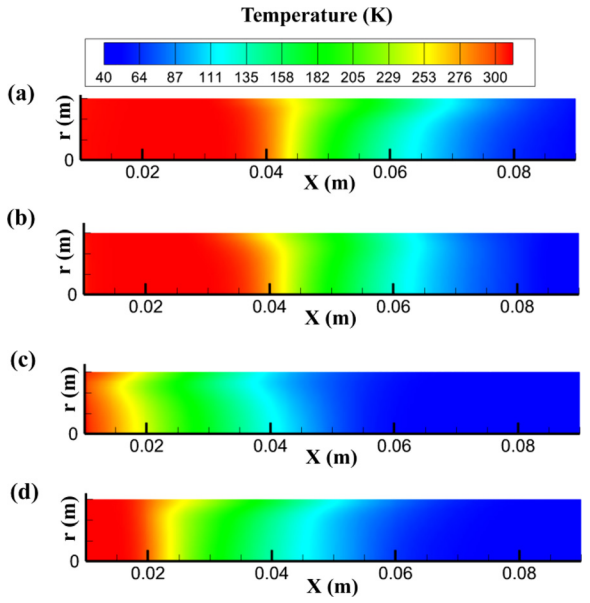

FIG. 8. Temperature contour inside the second-stage pulse tube for 4.0 W heat loads for a phase angle of (a) 0°, (b) 90°, (c) 180°, (d) 270°.

II. MODEL DEVELOPMENT AND SOLUTION APPROACH

A. Geometrical model description

The PTC comprises a compressor, regenerator, pulse tube, and three heat exchangers. The compressor provides high-pressure gas, which is cooled in the regenerator and expands in the pulse tube, resulting in temperature drop. In the two-stage coaxial PTC as illustrated in Fig. 1, the cold heat exchanger of the first stage is cascaded to the second stage though a thermal bridge and a middle heat exchanger. Thus, an additional cooling effect is provided to the second-stage gas parcel to further reduce the temperature. This is achieved through thermal coupling by which an energy exchange occurs, on the other hand, the fluid mass is isolated with respect to each stage separately.

In order to investigate the fluid flow and heat transfer characteristics of the PTC, axisymmetric models of first and second stage cryocoolers are designed and constructed by utilizing ANSYS DM® as shown in Figs. 2(a) and 2(b) respectively. The dimensional details of the cryocoolers are tabulated in Tables I and II respectively for first and second stages. These dimensions are considered and validated from the experimental works of Dang *et al.*[21] The coaxial configuration of the PTC is described as set of concentric cylinders with the inner one being the pulse tube and the outer cylinder being the regenerator. A quadrilateral structured mesh is utilized in order to discretize the

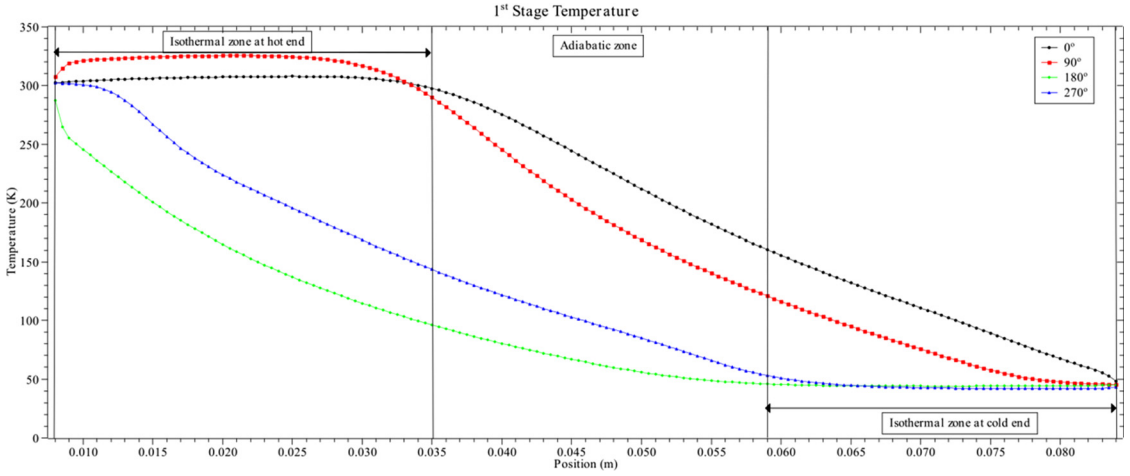

FIG. 9. Axial temperature distribution within the first-stage of pulse tube for 0.6 W heat load.

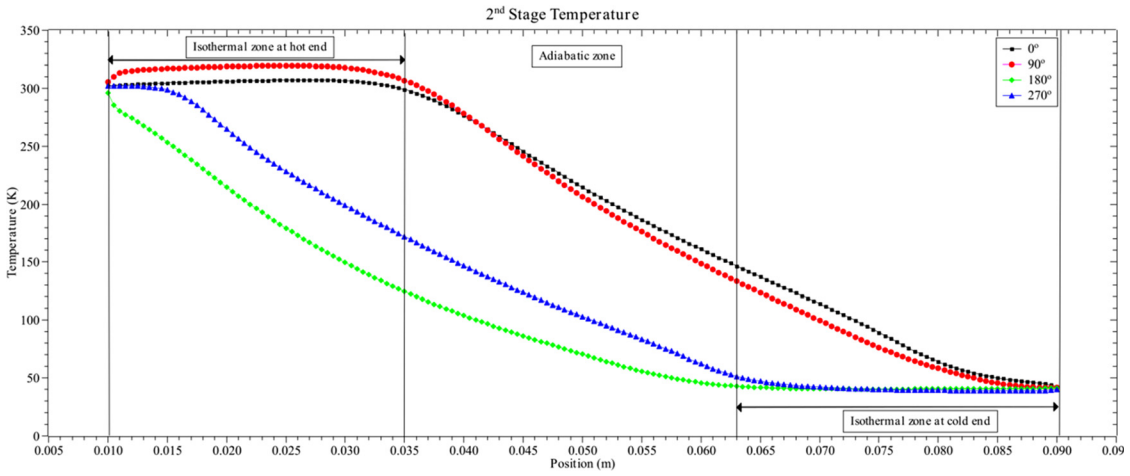

FIG. 10. Axial temperature distribution inside the second-stage pulse tube.

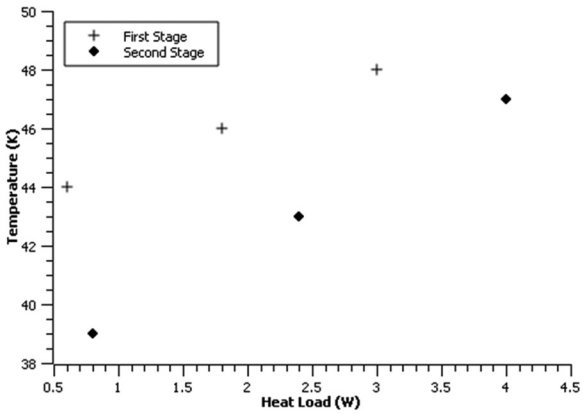

FIG. 11. Minimum refrigeration temperature in PTCs for different heat loads.

geometry into high quality rectangular elements. The number of elements with respect to each stage is denoted in Table III after conducting grid-independence test.

B. Boundary conditions for the domain

The PTC operates on a closed cyclic process as there is no mass transfer with respect to the atmosphere, but heat transfer happens at heat exchangers. For the purpose of simplifying the simulation and reducing the computational intensity, the input pressure wave is generated by using a "User Defined Function" in Fluent and is assigned as a boundary condition instead of geometrically modeling the compressor. The general form of the sinusoidal pressure equation is illustrated in Eq. (1). A frequency of 32 Hz is considered with a mean pressure of 13 bars and an amplitude of ±5 bars in these simulations,[12,13]

$$P_{\text{in}} = P_0 + P_a \sin(2\pi f t). \tag{1}$$

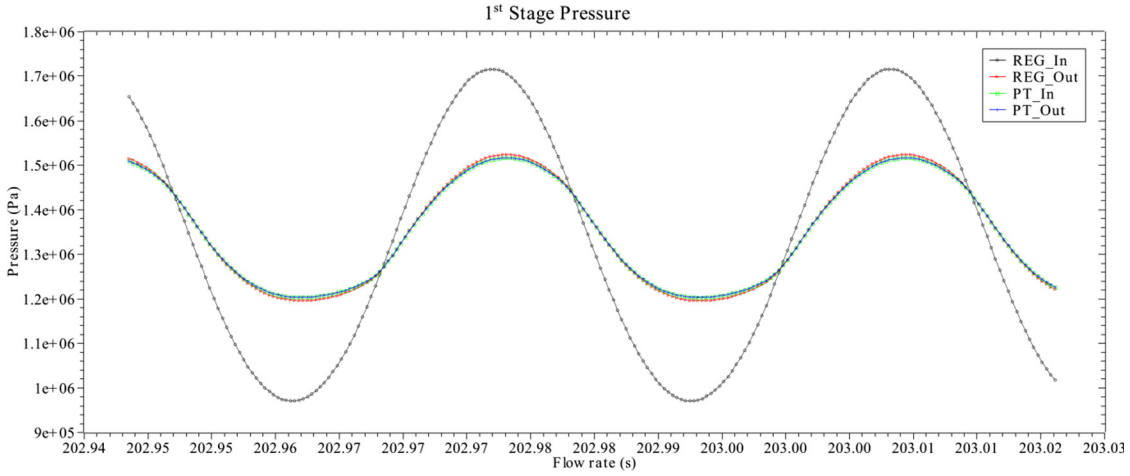

FIG. 12. Cyclic pressure distribution within the first stage.

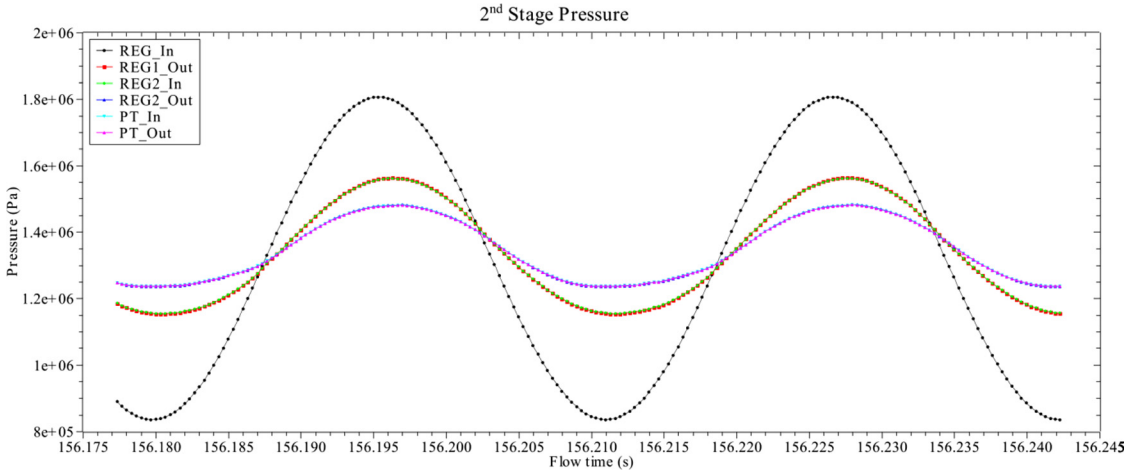

FIG. 13. Cyclic pressure distribution within the second stage.

Since the PTC is of coaxial type, the area between the concentric cylinders is modeled to be an adiabatic zone in order to eliminate any type of undesirable heat transfer that may occur between them. The boundary conditions of the remaining components in the system are tabulate as shown in Table IV. Heat exchangers and regenerators are modeled to be porous regions using the mathematically calculated values as tabulated in Table V.

C. Governing equations for numerical simulation

The axis-symmetric model solve the continuity, momentum and energy equations in order to calculate the heat transfer processes for a closed cycle and separate formulations are used for porous and non-porous zones.[19] Equations (2)–(4) represent the conservation equations for the non-porous zones in the thermal system.[19]

Continuity equation for non-porous zone is written as

$$\frac{\partial \rho_f}{\partial t} + \frac{1}{r}\frac{\partial}{\partial r}(r\rho_f v_r) + \frac{\partial}{\partial z}(\rho_f v_z) = 0. \tag{2}$$

Momentum equation for non-porous zone is written as

$$\frac{\partial}{\partial t}(\rho_f v_x) + \frac{\partial}{\partial z}(\rho_f \vec{v}\vec{v}) = -\nabla P + \nabla(\bar{\bar{\tau}}). \tag{3}$$

Energy equation for non-porous zone is written as

$$\frac{\partial}{\partial t}(\rho_f E_f) + \nabla.\left(\vec{v}(\rho_f E_f + P)\right) = \nabla.\left((k)_f \nabla T(\bar{\bar{\tau}} + \vec{v})\right). \tag{4}$$

Equations (5), (6), and (9) collectively describe the conservation of mass, momentum, and energy within a porous region, accounting for fluid flow, pressure gradient, viscous effect, and thermal processes when a local thermal equilibrium model is assumed for the porous domain.[19]

Continuity equation for porous zone is written as

$$\frac{\partial}{\partial t}(n_g \rho_f) + \frac{1}{r}\frac{\partial}{\partial r}(r n_g \rho_f v_r) + \frac{\partial}{\partial z}(n_g \rho_f v_z) = 0. \tag{5}$$

Momentum equation for porous zone is written as

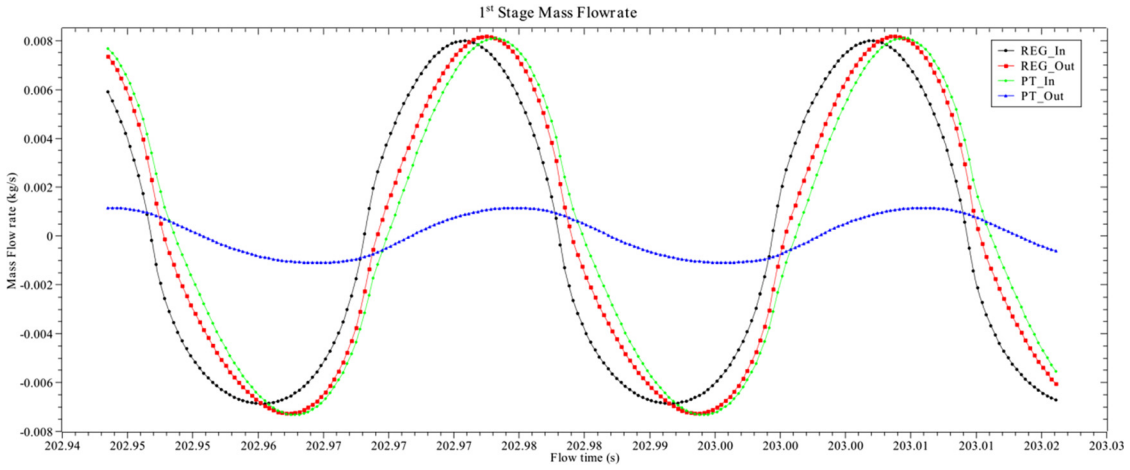

FIG. 14. Cyclic mass flow rate distribution within the first stage.

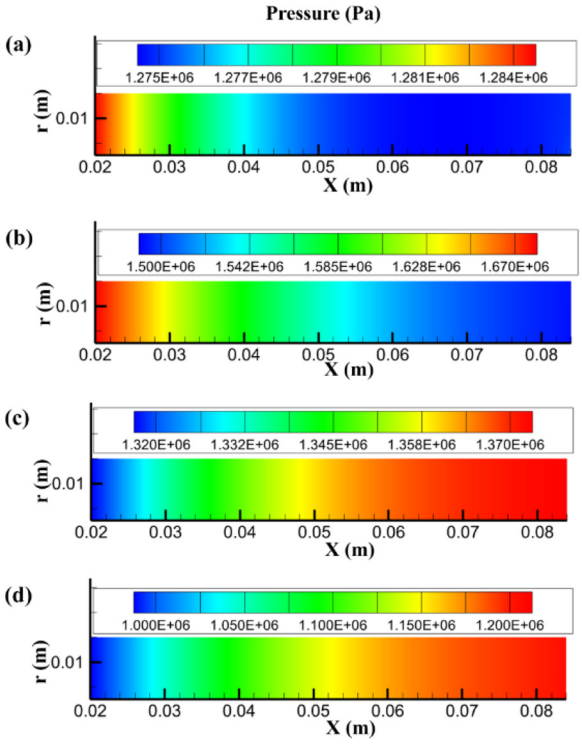

FIG. 15. Pressure contour within the first-stage regenerator for a phase angle of (a) 0°, (b) 90°, (c) 180°, and (d) 270°.

$$\frac{\partial}{\partial t}\left(n_g\rho_f\vec{v}\right)+\nabla.\left(n_g\rho_f\vec{v}\vec{v}\right)=-n_g\nabla P+\nabla.\left(n_g\bar{\bar{\tau}}\right)-\left(\mu\bar{\bar{\beta}}.\vec{j}+\frac{1}{2}\overline{\overline{C_2}}\rho_f|\vec{j}|\vec{j}\right),\quad(6)$$

where, the values for inertial resistance (C_2) factor and viscous resistance (β) are given by

$$C_2=\frac{3.5}{D_p}\frac{(1-n_g)}{{n_g}^3},\quad(7)$$

$$\beta=\frac{1}{\alpha}=\frac{D_h^2}{150}\frac{{n_g}^3}{(1-n_g)^2}.\quad(8)$$

Energy equation for porous zone is written as

$$\frac{\partial}{\partial t}\left(n_g\rho_f E_f+(1-n_g)\rho_s E_s+\nabla.\left(\vec{v}\left(\rho_f E_f+P\right)\right)\right)=\nabla.\left(\left(n_g(k)_f+(1-n_g)(k)_s\right)\nabla\mathrm{T}+\left(n_g\bar{\bar{\tau}}.\vec{v}\right)\right).\quad(9)$$

D. Details of simulation method

CFD simulation is conducted using Ansys Fluent® by focusing on the transient behavior of a system. This is carried out by using a segregated pressure-based solver. The study investigates the use of ideal helium gas as the working fluid, with copper and steel employed as the solid materials in the heat exchangers and nonporous zones of the computational domain respectively.

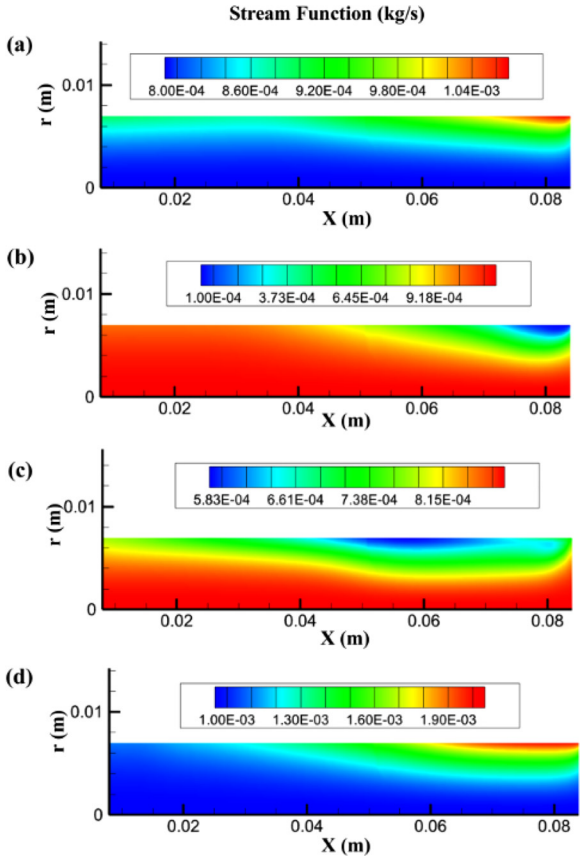

FIG. 16. Stream function contour within the first-stage pulse tube for 0.6 W of heat load for a phase angle of (a) 0°, (b) 90°, (c) 180°, and (d) 270°.

The simulation incorporates an absolute velocity formulation and a porous formulation using superficial velocity. The SIMPLE scheme is employed with the standard option chosen for pressure calculation, and second-order upwind methods are chosen for density and momentum calculations. To ensure accurate results, appropriate under relaxation factors are applied. The convergence criteria for energy equation are set at 1×10^{-6}, while the value for continuity, r-velocity, z-velocity, k, and ε, is chosen as 1×10^{-3}. The time step size is set to 0.001, allowing for a maximum of 50 iterations per time step. The simulation is performed for a total of 600 000 time steps, aiming to capture the transient behavior of the system accurately from ambient temperature initial condition.

III. RESULTS AND DISCUSSION

The cooling principle behind the PTC involves the utilization of oscillating pressure waves within a hollow tube to generate a temperature gradient. In a PTC, the temperature distribution within the pulse tube plays a crucial role in determining the cooling performance and efficiency of the system. The variation of temperature of the first stage pulse tube at four different phase angles of the cycle (0°, 90°, 180°, and 270°) is shown in Figs. 3–5 for heat load values of 0.6 W, 1.8 and 3 W at the cold heat exchangers respectively. The thermal distribution

length of the warmer end of the pulse tube is observed to be more during compression and conversely the length of the colder end of the pulse tube is greater during expansion. The temperature distribution is influenced by various factors, including the gas flow dynamics, heat transfer mechanism, regenerator design, and the presence of gas streaming effects. A similar temperature representation of the second stage pulse tube is illustrated in Figs. 6–8 for the heat load values of 0.8 W, 2.4 and 4 W respectively. When the gas is compressed into the pulse tube, a rise in temperature can be observed during pressurization, whereas during the expansion process of the cycle, temperature drops near the cold end which can be observed in Figs. 3–5 for the first stage, and Figs. 6–8 for the second stage PTC's. This observation is similar those of earlier researchers.[11,15] This temperature gradient occurs along the axial line due to surface heat pumping principle as illustrated by Longworth and Gifford.[20] The temperature distribution along the length of the pulse tube is represented in Fig. 9 for the first stage and in Fig. 10 for the second stage respectively for different flow times. These figures show the formation of axial temperature gradient from the cold end of the pulse tube toward its hot end. During the compression stage, axial temperature is constant near the hot end and gradually decreases to the lowest point toward the cold end. Inversely, during the expansion, the temperature value reduces directly from the hot end and is observed to be constant near the cold end. Figure 11 illustrates the minimum cold end temperature achieved by both the first and second stage PTC for different heat loads. A temperature of 39 K is achieved in the two-stage PTC for a heat load of 0.8 W.

Due to the porous nature of the regenerator, a pressure drop is observed when the flow occurs through it. This is shown in Fig. 12 for the first stage and Fig. 13 for the second stage of simulated PTC. The pressure drops across the pulse tube in both the first and second stages is negligible as it is a non-porous zone, and a similar explanation was noticed earlier.[11,15] Figure 14 represents the phase difference in the mass flow across the regenerator and pulse tube of the first stage PTC. Mass flow at the regenerator outlet leads the mass flow at inlet, which is primarily due to the storage and release of thermal energy during the operation of the system. The thermal inertia of the solid matrix results in a delay of heat transfer between the solid and the fluid. This causes the fluid mass flow at the outlet of the regenerator to experience an increase in temperature before the fluid at the regenerator inlet. This also leads to a phase lead in mass flow and temperature at the outlet compared to the inlet. A pressure drop of around 2 bars is observed between the inlet and outlet of the first stage regenerator. The mass flow is observed to be in phase with respect to regenerator outlet and pulse tube inlet. Figure 15 shows the variation of pressure in the first

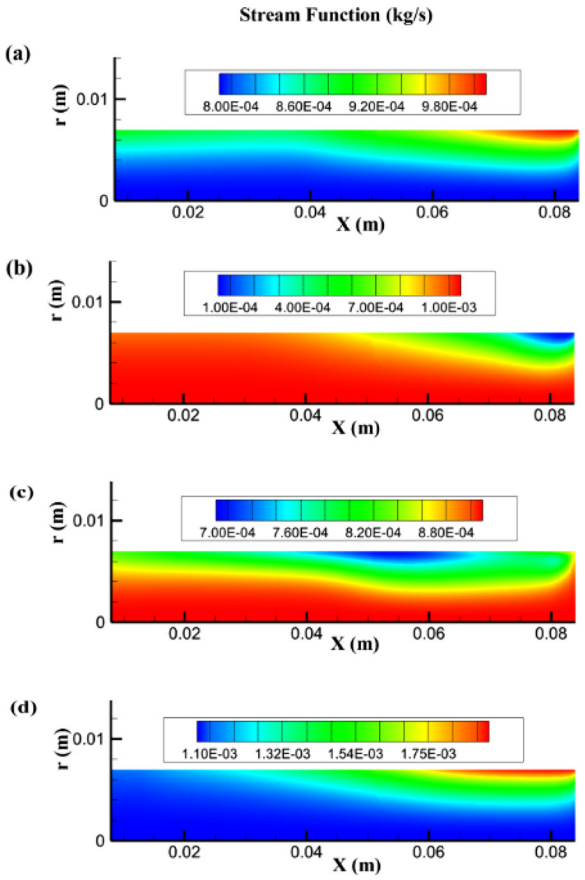

FIG. 17. Stream function contour within the first-stage pulse tube for 1.8 W of heat load for a phase angle of (a) 0°, (b) 90°, (c) 180°, and (d) 270°.

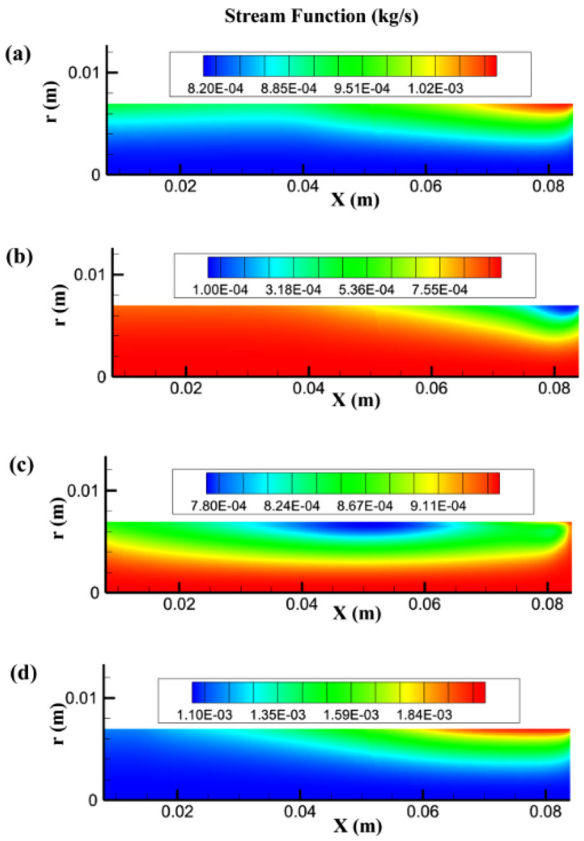

FIG. 18. Stream function contour within the first-stage pulse tube for 3.0 W of heat load for a phase angle of (a) 0°, (b) 90°, (c) 180°, and (d) 270°.

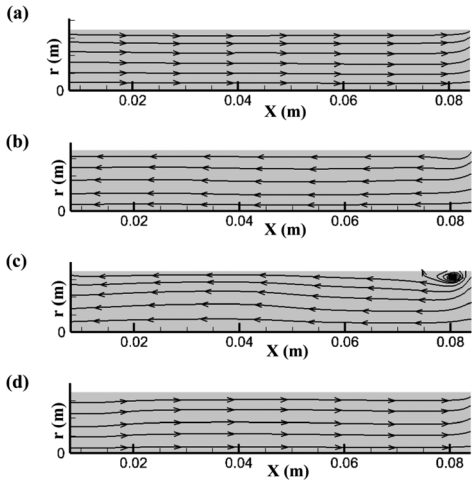

FIG. 19. Stream line plots within the first-stage pulse tube for 0.6 W of heat load for a phase angle of (a) 0°, (b) 90°, (c) 180°, and (d) 270°.

stage regenerator, and a linear pressure gradient is observed for the compression and expansion stages of the working cycle.

Figures 16–18 illustrate the stream function of the working fluid in the first stage pulse tube and the contours are plotted for every quarter phase angle to study its variation during both compression and expansion of gas parcels. The stream function is a scalar function that represents the flow pattern in a two-dimensional plane perpendicular to the direction of flow. It provides information about the direction and strength of the fluid motion. Similarities can be observed for the angles of 0° and 270° and a higher value is observed near the cold end and top part of the pulse tube. In the case of 90° and 180° phase angles,

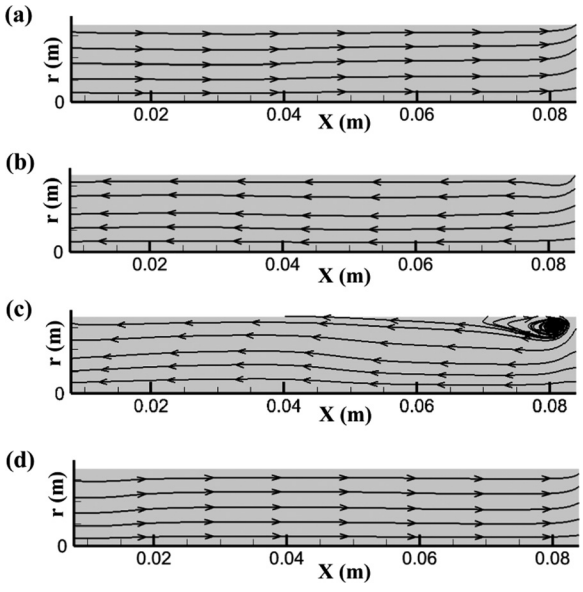

FIG. 20. Stream line plots within the first-stage pulse tube for 1.8 W of heat load for a phase angle of (a) 0°, (b) 90°, (c) 180°, and (d) 270°.

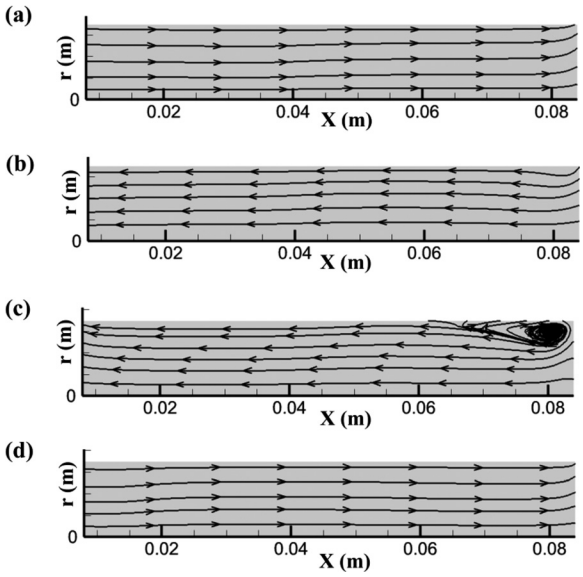

FIG. 21. Stream line plots within the first-stage pulse tube for 3.0 W of heat load for a phase angle of (a) 0°, (b) 90°, (c) 180°, and (d) 270°.

a reverse trend can be observed and this cycle repeats throughout the working of the PTC. Maximum variation is detected at 180° phase angle in which a continuous propagation is observed throughout the length of the pulse tube. The stream function is particularly used to analysis pulse tube's flow field description, which allows for a better understanding of the complex fluid dynamics involved in the generation of vortices and flow separation. The flow behavior is further visualized by plotting streamlines as shown in Figs. 19–21 for varying heat loads of the first stage pulse tube. Streamlines are curves or tangents to the velocity vector through which the flow patterns and fluid circulations are captured in the pulse tube. The streamlines plotted in Figs. 19–21 showcases the vortex formations at 180° phase angle of the cycle whereas linear flow is observed at other instances. The size of the vortex is observed to increase in diameter and length for an increment in cold end heat load, thus showcasing the physics for a drop in performance when subjected to higher heat capacities.

IV. CONCLUSIONS

In this paper, a numerical investigation is conducted for two-stage coaxial pulse tube cryocooler for the first-time and the results obtained from the analysis provide valuable insights into its cooling performance and efficiency. The presence of vortices and flow separation within the pulse tube was visualized using streamlines, highlighting the complex fluid dynamics involved behind its formulation. Vortex formations were observed at specific phase angles of the cycle, particularly at the 180° angle. The size and extent of these vortices increased with higher heat loads, indicating a drop in performance under higher heat capacities. The temperature distribution within the pulse tube plays an important role in determining the cooling behavior of the system. It was observed that during compression, the axial temperature remains relatively constant near the hot end and gradually decreases toward the cold end, while during expansion, the temperature decreases directly from the hot end and remains relatively

constant near the cold end. The regenerator, composed of a porous material, played a crucial role in enhancing the cooling process. A pressure drop was observed across the regenerator due to the flow through its porous structure, while the pressure drop across the non-porous pulse tube was negligible. Overall, these findings contribute to a better understanding of the flow physics and fluid dynamics of pulse tube cryocoolers. They provide valuable insights for optimizing the design, efficiency, and cooling performance of PTC systems in various applications.

Further studies and improvements based on these results can lead to advancements in pulse tube technology and its applications in real world problems.

AUTHOR DECLARATIONS

Conflict of Interest

The authors have no conflicts to disclose.

Author Contributions

Damu C.: Conceptualization (lead); Data curation (lead); Formal analysis (equal); Investigation (lead); Methodology (equal). **Sumukh Moudghalya:** Conceptualization (equal); Data curation (equal); Formal analysis (equal). **Mrunal Nerale:** Conceptualization (equal); Data curation (lead); Formal analysis (equal); Investigation (equal). **Debashis Panda:** Conceptualization (supporting); Data curation (supporting); Formal analysis (equal); Investigation (supporting). **Rajendra Prasad K. S.:** Conceptualization (equal); Data curation (equal); Formal analysis (equal); Investigation (lead); Methodology (equal). **Upendra Behera:** Conceptualization (equal); Data curation (equal); Formal analysis (supporting); Investigation (equal); Methodology (equal). **Sathyanarayana Reddy:** Conceptualization (supporting); Data curation (supporting); Formal analysis (supporting); Investigation (equal); Methodology (supporting).

DATA AVAILABILITY

Data sharing is not applicable to this article as no new data were created or analyzed in this study.

REFERENCES

[1]R. Radebaugh, "Cryocoolers: The state of the art and recent developments," J. Phys.: Condens. Matter **21**, 164219 (2009).

[2]V. S. Chakravarthy, R. K. Shah, and G. Venkatarathnam, "A review of refrigeration methods in the temperature range 4–300 K," J. Therm. Sci. Eng. Appl. **3**, 020801 (2011).

[3]J. Pfotenhauer, R. Wang, and F. Miller, "Regenerator design optimization: Results from REGEN 3.3," Cryogenics **97**, 77 (2019).

[4]J. M. Pfotenhauer, Z. H. Gan, and R. Radebaugh, *Approximate Design Method for Single Stage Pulse Tube Refrigerators* (American Institute of Physics, Melville NY, 2008).

[5]R. Snodgrass, J. Ullom, and S. Backhaus, *Optimal Absorption of Distributed and Conductive Heat Loads with Cryocooler Regenerators* (IOP Publishing, 2022).

[6]T. Tsukagoshi, K. Matsumoto, T. Hashimoto, T. Kuriyama, and H. Nakagome, "Optimum structure of multilayer regenerator with magnetic materials," Cryogenics **37**, 11 (1997).

[7]D. Panda, M. Kumar, A. K. Satapathy, and S. K. Sarangi, "Optimal design of thermal performance of an orifice pulse tube refrigerator," J. Therm. Anal. Calorim. **143**, 3589 (2021).

[8]D. Panda, A. K. Satapathy, and S. K. Sarangi, "Thermoeconomic performance optimization of an orifice pulse tube refrigerator," Sci. Technol. Built Environ. **26**, 492 (2020).

[9]C. Gu, Y. Zhou, J. Wang, W. Ji, and Q. Zhou, "CFD analysis of nonlinear processes in pulse tube refrigerators: Streaming induced by vortices," Int. J. Heat Mass Transfer **55**, 7410 (2012).

[10]W. Liang and A. de Waele, "A new type of streaming in pulse tubes," Cryogenics **47**, 468 (2007).

[11]D. Panda, A. K. Satapathy, and S. K. Sarangi, "Effect of thermal dispersion and turbulent conduction on the heat transfer behavior of coaxial pulse tube cryocooler," Numer. Heat Transfer, Part A **83**(12), 1303–1330 (2023).

[12]Y. Zhao and H. Dang, "CFD simulation of a miniature coaxial Stirling-type pulse tube cryocooler operating at 128 Hz," Cryogenics **73**, 53 (2016).

[13]Y. Zhao, G. Yu, J. Tan, X. Mao, J. Li, R. Zha, N. Li, and H. Dang, "CFD modeling and experimental verification of oscillating flow and heat transfer processes in the micro coaxial Stirling-type pulse tube cryocooler operating at 90–170 Hz," Cryogenics **90**, 30 (2018).

[14]Q. Zhou, L. Chen, X. Zhu, W. Zhu, Y. Zhou, and J. Wang, "Development of a high-frequency coaxial multi-bypass pulse tube refrigerator below 14 K," Cryogenics **67**, 28 (2015).

[15]D. Panda, A. K. Satapathy, and S. K. Sarangi, "Influence of gas axial conduction enhancement factor on the oscillating flow behavior of an inertance pulse tube cryocooler," Cryogenics **122**, 103437 (2022).

[16]T. Fang, T. Mulcahey, R. Taylor, P. Spoor, T. Conrad, and S. Ghiaasiaan, "Method for estimating off-axis pulse tube losses," Cryogenics **88**, 1 (2017).

[17]T. Fang, P. Spoor, and S. Ghiaasiaan, *A Computational Approach for Coupled 1D and 2D/3D CFD Modelling of Pulse Tube Cryocoolers* (IOP Publishing, 2017).

[18]T. I. Mulcahey, "Convective instability of oscillatory flow in pulse tube cryocoolers due to asymmetric gravitational body force," Ph.D. thesis (Georgia Institute of Technology, 2014).

[19]D. Panda, M. Kumar, A. K. Satapathy, S. Sarangi, and U. Behera, "Investigations on nonlinear processes of a Gifford-McMahon type orifice pulse tube refrigerator," Proc. Inst. Mech. Eng., Part E (published online, 2023).

[20]W. E. Gifford and R. C. Longsworth, *Surface Heat Pumping* (Springer, Boston, MA, 1966).

[21]H. Dang, R. Zha, J. Tan, T. Zhang, J. Li, N. Li, and R. Xue, "Investigations on a 3.3 K four-stage Stirling-type pulse tube cryocooler. Part B: Experimental verifications," Cryogenics **105**, 103015 (2020).